TEST OF MODELS FOR REPLICATION OF SIMIAN VIRUS 40 DNA FOLLOWING ULTRAVIOLET IRRADIATION

Susan W. Barnett
The Molecular Biology Institute, University of California, Los Angeles, California 90024

Elliot M. Landaw
Departments of Biomathematics and Pediatrics, University of California, Los Angeles, California 90024

Kathleen Dixon
The Department of Biological Chemistry and the Molecular Biology Institute, University of California, Los Angeles, California 90024

ABSTRACT When mammalian cells are irradiated with ultraviolet light, semiconservative DNA replication is inhibited and the length of newly synthesized daughter strands is reduced. We have used the simian virus 40 (SV40) viral system to examine the molecular mechanism by which this inhibition of DNA replication occurs immediately following ultraviolet irradiation. We tested two models for DNA replication-inhibition by using a procedure first developed by Danna, K. J., and D. Nathans (1972, *Proc. Natl. Acad. Sci. USA*, 69:3097–3100) in which the distribution of ^{3}H-label in segments of newly completed SV40 form-I molecules is measured after short pulse labeling with ^{3}H-thymidine. Our experimental results were compared with those predicted by mathematical models that describe two possible molecular mechanisms of replication inhibition. Our data are best fit by a "blockage" model in which any pyrimidine dimer encountered by the replication fork prevents complete replication of the SV40 genome. An alternative model called "slowdown" in which DNA damage causes a generalized slowdown of replication fork movement on all genomes has more adjustable parameters but does not fit the data as well as the blockage model.

INTRODUCTION

When mammalian cells are irradiated with ultraviolet (UV) light, subsequent semiconservative DNA replication is inhibited (for review, see Hall and Mount, 1981). The reduction in the rate of DNA replication is UV-fluence dependent and, at higher fluences (>5 J/m^2), the rate of replication continues to decrease as a function of time for at least 1 h following irradiation (Dahle et al., 1980; Stacks, et al., 1983). The kinetics of recovery of DNA synthesis following UV irradiation also appear to be fluence dependent; for fluences >10 J/m^2, the DNA synthesis rate of HeLa cells does not appear to recover for up to 6 h after UV irradiation (Edenberg, 1976).

Two different types of models have been proposed to explain this inhibition of DNA replication: (*a*) "lesion-specific blockage" in which UV-induced damage in DNA interferes with replication directly by (*i*) causing replication forks to pause or stop at damage sites or (*ii*) causing gaps to be left in daughter strands opposite the damage sites; (*b*) "nonlesion-specific slowdown" in replication fork progression or strand joining due to cell-wide effects of DNA damage on the replication machinery. Data supporting the first of these two types of models have been derived from three main types of experiments: (*a*) measurements of the rate of incorporation of ^{3}H-thymidine into total cellular DNA (Edenberg, 1976; Doniger, 1978), (*b*) measurements of the size distribution of newly synthesized DNA strands on alkaline sucrose gradients (see e.g., Lehmann, 1972; Doniger, 1978), and (*c*) measurements of the length of segments of newly synthesized DNA by fiber autoradiography (Edenberg, 1976; Dahle et al., 1980; Doniger, 1978). The results of these experiments indicate that there is a correlation between the number of pyrimidine dimers introduced into the DNA and the overall reduction in DNA synthesis, the size of newly synthesized single strands, and the length of newly replicated DNA segments, which suggests lesion-specific blockage. However, interpretation of these studies and further confirmation of the models are complicated by the fact that replication in mammalian cells normally occurs on a heterogeneous population of replicons, and the population

of active replicons may change after UV irradiation. Many of the results could be explained equally well by a nonspecific, generalized slowdown in the rate of replication fork movement and/or in the rate of joining of Okazaki fragments and replicons. These more generalized effects on replication in UV-damaged cells might occur if, for example, components of the replication apparatus were being used for DNA repair processes and were less available for semiconservative DNA replication (Hall and Mount, 1981).

To avoid some of the problems that arise in the study of cellular genomic DNA, we have chosen to study the replication of UV-damaged simian virus 40 (SV40) DNA in its mammalian host, the African green monkey kidney cell line TC7. The circular SV40 viral DNA is replicated bidirectionally from a unique origin by the host cell's replication machinery (for review, see DePamphilis and Wassarman, 1982). Termination occurs when the replication forks meet (~180° around the circle from the origin) and two, closed circular supercoiled form-I daughter molecules are produced. A single replication cycle normally takes ~15 min (Danna and Nathans, 1972). By using this well-defined viral system, we are able to examine in detail the effects of UV damage on DNA replication on the molecular level. Previous studies in our laboratory (Stacks et al., 1983) and others (Edenberg, 1983; Sarasin and Hanawalt, 1980; Williams and Cleaver, 1978) have indicated that, like cellular DNA replication, viral DNA replication is inhibited by UV irradiation in a fluence-dependent fashion. Furthermore, newly replicated strands have a size distribution that correlates with the interdimer distance (Sarasin and Hanawalt, 1980). Here again, it has been proposed that the reduction in DNA replication is due to lesion-specific blockage.

To test the existing models for inhibition of DNA replication by UV radiation more rigorously, we have made use of a technique developed by Danna and Nathans (1972) for measuring the time required to replicate the SV40 viral genome. SV40-infected cells are pulse labeled with ^{3}H-thymidine for short periods (less than or equal to the time required for one round of replication), and the distribution of label in completed molecules is determined following restriction cleavage of purified SV40 form-I DNA. For the shortest pulse times, segments of the DNA located nearest the terminus of replication are labeled almost exclusively. As the duration of the pulse label increases and approaches the average time required to replicate the entire SV40 genome, the label in origin-proximal segments increases, and the label intensity in a segment becomes proportional to the distance of the segment from the origin.

We have combined the Danna and Nathans technique with mathematical modeling and model fitting to address the following specific questions. (a) Can inhibition of replication of UV-damaged DNA be described adequately by a lesion-specific blockage model (i) in which strand

elongation is blocked (either by the replication fork stopping or pausing or by gap formation) at the sites of UV damage in the DNA and (ii) in which undamaged molecules and molecules with damage sites behind the replication fork continue to replicate at the normal rate? (b) Can a mathematical model be derived to adequately describe replication of UV-damaged SV40 DNA in terms of the nonspecific slowdown model in which both UV-damaged and -undamaged molecules replicate more slowly than normal? (c) Is it possible to distinguish between these two models on the basis of their fit to results from Danna and Nathans-type experiments?

METHODS

Cell Culture

African green monkey kidney cells (the TC7 clone of the CV-1 line; Robb and Huebner, 1973) were routinely grown in minimal essential medium with Earles salts (Gibco Laboratories, Grand Island, NY), supplemented with 5% calf serum (Gibco Laboratories), 100 units/ml penicillin, and 100 μg/ml streptomycin. Cells were kept at 5% CO_2 in a humidified atmosphere at 37°C.

Virus Stocks

SV40 virus (wild type 830; Shenk et al., 1976) was prepared by infection of subconfluent TC7 cells with plaque-purified SV40 virus at a multiplicity of infection (MOI) of 0.001 plaque-forming unit (PFU) per cell. The virus was prepared from infected cell cultures after 10–14 days and concentrated by virus adsorption-deadsorption (Diggelmann and Beard, 1976) and low-speed centrifugation followed by three consecutive rounds of freezing in an ethanol/dry-ice bath (−70°C) and thawing in a 37°C water bath. Virus stocks were subsequently titrated by plaque assay.

Infection of Cells

For each experiment, cells were plated in plastic 100-mm culture dishes at ~⅛ of the confluent cell density. After 2 d of incubation, subconfluent cultures were infected with SV40 at an MOI of 1–5 PFU per cell. Experiments were performed 38–40 hours after infection at a time when viral DNA synthesis was maximal.

UV Irradiation and Cell Labeling

Medium was aspirated from infected cells just before UV irradiation. Cells were rinsed with prewarmed (37°C) phosphate-buffered saline (PBS; 8 g NaCl, 0.2 g KCl, 1.15 g Na_2HPO_4 · $7H_2O$, 0.2 g KH_2PO_4/ liter), overlayed with 5 ml warm PBS, and irradiated. Cells were irradiated for 60 to 90 s with a low-pressure mercury lamp emitting maximally at 254 nm with a fluence rate of 0.66 J/m^2/s as determined by potassium ferrioxalate actinometry (Jagger, 1967). Under the conditions of our experiments, a fluence of 20 J/m^2 introduces an average of about one pyrimidine dimer per SV40 genome (Stacks et al., 1983). The PBS overlay was removed immediately after UV irradiation, and the cells were covered with 1 ml of warm conditioned medium (taken from experimental dishes before the experiment) and then pulse labeled with 150 μCi ^{3}H-thymidine (50–100 Ci/mmol, New England Nuclear, Boston, MA or Amersham Corp., Arlington Heights, IL) for the indicated periods of time. During the pulse, the dishes of cells were floated on a water bath at 37°C in a 5% CO_2 humidified atmosphere. At the end of the pulse, labeled medium was removed, cells were rinsed two times with cold PBS, and 0.8 ml of Hirt extraction buffer (0.6% sodium dodecyl sulfate [SDS], 10 mM Tris-HCl, 10 mM EDTA, pH 7.5 [Hirt, 1967]) was added to each dish. After an incubation time >10 min, the lysed cells from each dish were

scraped into 15-ml corex tubes containing 0.2 ml 5 M NaCl for extraction of viral DNA. Control dishes were treated identically except infected cells were not UV irradiated.

Purification of Form-I SV40 DNA

Hirt supernatants from three to seven replicate dishes were pooled, and CsCl and ethidium bromide were added to yield a final density of ~1.57 g/cc and a final concentration of 100 μg/ml, respectively. CsCl-ethidium bromide gradients were centrifuged at 38,000 rpm for 60 h in a Ti 50 rotor (Beckman Instruments, Inc., Fullerton, CA). Form-I DNA-containing fractions were pooled, ethidium bromide was removed by n-butanol extraction, and samples were dialyzed extensively against 0.3 M NaCl, 10 mM Tris-HCl, 1 mM EDTA, pH 7.5, for subsequent benzoylated napthoylated DEAE (BND)-cellulose (Sigma Chemical Co., St. Louis, MO) chromatography. Samples were applied to BND-celulose columns, and form-I SV40 DNA was purified away from any residual replicative intermediate molecules by elution from the column in a buffer containing 0.65 M NaCl, 10 mM Tris-HCl, 1 mM EDTA, pH 7.5. Form-I DNA-containing fractions were pooled, dialyzed, ethanol precipitated, and the DNA was resuspended in a buffer containing 10 mM Tris-HCl, 1 mM EDTA, pH 7.5 (TE). An aliquot was electrophoresed on a 1% agarose gel to assess the concentration, purity, and specific activity (counts per minute per microgram) of form-I SV40 DNA samples.

Preparation of Uniformly Labeled ^{32}P-SV40 DNA

SV40-infected cells were labeled with 30 μCi/ml ^{32}P-orthophosphate (ICN) beginning 24 h after infection. Form-I viral DNA was isolated at 60–65 h after infection by Hirt extraction (Hirt, 1967) followed by CsCl-ethidium bromide gradient banding as described above.

Restriction Analysis of Form-I SV40 DNA

^{3}H-thymidine-labeled DNA samples were mixed with uniformly labeled ^{32}P-SV40 DNA such that the ^{3}H/^{32}P ratio was >5. These samples were digested with a five-fold excess of HindII and HindIII restriction endonucleases (Bethesda Research Laboratories, Gaithersburg, MD). DNA fragments were separated on 4% acrylamide gels as described by Danna and Nathans (1972). DNA bands, located by autoradiography of the wet gel (using Kodak XAR film; Eastman Kodak, Rochester, NY), were cut out. The gel slices were solubilized by the addition of 0.5 ml 30% H_2O_2 and 5 μl NH_4OH followed by heating at 100°C for 30–45 min and ^{3}H and ^{32}P radioactivity was determined by scintillation counting.

Determination of Yield of ^{3}H Label in Form–I-completed Molecules

The total yield of ^{3}H label in form-I molecules was determined for each experiment by using a ^{32}P-prelabel as an internal standard for total SV40 DNA. Infected cells were labeled with ^{32}P-orthophosphate (0.5 μCi/ml) from 24 to 37 h after infection; ^{32}P-labeled medium was removed from the cells at least 1 h before the experiment was initiated. Prelabeled samples were treated under the same experimental conditions as samples used for purification of form-I DNA for later restriction analysis. For experiments 1 and 2, the yield of ^{3}H-label in form-I SV40 DNA was measured as the ratio of ^{3}H to ^{32}P radioactivity in form-I DNA bands taken from 1% agarose gels of Hirt-extracted viral DNA. Hirt supernatants were treated with RNase A and protease K, and ethanol precipitated before gel electrophoresis. All yield values are expressed as the percentage of the yield for the unirradiated control sample of the longest pulse duration (for each separate experiment). For experiment 3, the yield was measured as the actual specific activity (^{3}H cpm/ug DNA determined by A_{260}) of purified form-I SV40 DNA samples before restriction analysis. As a check on the ^{32}P-prelabeling method of determining yield, the yield of

^{3}H-label in form I for experiment 3 was also measured employing a ^{32}P-prelabel as described above. These two separate methods of determination gave comparable values.

Entry of ^{3}H-Thymidine into Cells

SV40-infected cells were irradiated or mock treated as described above and then pulse labeled with 20 μCi/ml ^{3}H-thymidine (12.66 Ci/mmol, conditions chosen to approximate thymidine concentration, 1–2 × 10^{-6} M, employed during our experiments). At the end of each pulse, medium was removed and cell monolayers were rinsed four times with ice cold PBS to remove adherent extracellular radioactivity (Hand, 1976). Acid-soluble radioactivity was extracted from cells with 0.5 ml of 0.5 N perchloric acid (PCA) for 10 min on ice. Acid precipitable material was removed by centrifugation and the acid soluble fraction was neutralized by the addition of 1.4 N KOH. After 5 min on ice, extracts were again centrifuged to remove KClO$_4$ precipitates. ^{3}H-label in aliquots of these extracts was determined by scintillation spectrometry. Additional aliquots were taken for polyethyleneimine-(PEI-) cellulose chromatography to measure phosphorylation of exogenous thymidine.

PEI-Cellulose Chromatography

PEI-cellulose sheets (Brinkmann Instruments, Inc., Westbury, NY) were prerun by ascending chromatography with 1.5 M KH$_2$PO$_4$ and then submerged in a large volume of 0.05 M KH$_2$PO$_4$ for at least 1 h. Pretreated sheets were allowed to dry at room temperature and were subsequently used in ascending chromatography in the original direction. Aliquots of PCA extracts were spotted along with thymidine and thymidine nucleotide markers, and developed with 0.1 M KH$_2$PO$_4$ for 30 min and then 0.5 M KH$_2$PO$_4$ until the solvent front reached ~15.5 cm. Chromatograms were air-dried and markers were visualized by using UV light (254 nm) with fluorescent indicator-backed PEI-cellulose plates. Chromatographic lanes were cut into 0.5-cm strips, and thymidine and thymidine nucleotides were eluted by placing each strip in a scintillation vial and soaking each in 0.5 ml 0.7 M MgCl$_2$, 0.02 M Tris-HCl, pH 7.4, for 30 min at room temperature (Randerath and Randerath, 1968). Radioactivity in each strip was then determined by scintillation spectrometry after addition of 5-ml scintillation fluid.

Assay of Cellular Thymidine 5′-Triphosphate (dTTP)

Acid soluble extracts were prepared from mock-treated and irradiated SV40-infected cells essentially as described above with the following modifications. Pulses were performed with nonradioactive thymidine at 1.6 × 10^{-6} M. Cells were collected by scraping into PBS and centrifugation before PCA treatment. PCA precipitates were frozen for later protein determination (Lowry, 1951). Acid soluble extracts were neutralized, centrifuged, and stored at −70°C until the time of assay for dTTP.

Assay of the total cellular dTTP pool was performed by using Escherichia coli (E. coli) DNA polymerase I to measure limiting dTTP concentrations in acid extracts (Lindberg and Skoog, 1970). Thawed extracts were recentrifuged to remove residual KClO$_4$, made 0.01 M in potassium phosphate (pH 7.4), and subsequently treated with sodium periodate and methylamine-PO$_4$ (pH 7.5) to destroy ribonucleotides (Garrett and Santi, 1979). Without such treatment, we found it impossible to use DNA polymerase I to assay for dTTP in these extracts. Aliquots of each extract were assayed in a reaction mixture (0.2 ml) containing 0.05 M Tris-HCl (pH 8.0), 0.005 M MgCl$_2$, 0.01 M dithiothreitol, 200–300 pmol of dATP, dGTP, and dCTP, 1–2 × 10^6 dpm of α^{32}P-dCTP (500–1,000 Ci/mmol; Amersham Corp.), 0.45 U of E. coli DNA polymerase I (Boehringer Mannheim Biochemicals, Indianapolis, IN), 50 μg/ml of activated calf thymus DNA (100 μg/ml treated with 10 ng/ml DNase I at 37°C for 15 min and then 10 min at 65°C [Hand, 1976]). The polymerase reactions were allowed to proceed for 30 min at 37°C at which time 0.05-ml aliquots were removed from each and TCA

precipitated. The precipitates were collected on filters and ^{32}P-label was determined by scintillation spectrometry.

Data Analysis

Each of three experiments in this study comprised a collection of Danna and Nathans-type subexperiments along with determinations of total yield of form-I molecules. Each subexperiment was distinguished by its pulse-label duration and UV irradiation fluence (see Table I). For example, experiment 1 consisted of a control subexperiment (pulse label 15 min, no UV) and a second subexperiment (pulse label 15 min, UV irradiation 20 J/m^2). The observed ^{3}H/^{32}P ratios for each restriction fragment in a subexperiment and the relative yield of total label between subexperiments were combined in the following manner. Within each subexperiment, the observed ^{3}H/^{32}P ratio for a fragment was multiplied by its map length (see Appendix) to give the amount of ^{3}H-label in the fragment, and then normalized so that the sum of the fragment labels was equal to the observed total yield of label in form-I molecules expressed as a percentage of the control subexperiment of the longest pulse-label duration. These normalized total fragment yields were then divided by fragment map length to convert to (normalized) fragment label intensity (^{3}H label per size). This normalization allows the total yield information to be recovered from comparisons across subexperiments. An evaluation of the residuals in the subsequent model fitting process suggests that this did not introduce any significant correlated errors.

The main goal of the data analysis was to test how well the models fit the data for each experiment. The fitting of each model required the estimation of several model parameters (e.g., means and standard deviations of replication times), and the technique of weighted least squares was used for the simultaneous task of model fitting and parameter estimation. For fitting a model to an experiment, we chose model parameters that minimized the weighted sum of squared deviations (see below) between predicted and observed normalized fragment label intensities.

Model Fitting

Since the data from one or more subexperiments could be used to estimate the model parameters, two types of model fitting were performed for each of the three experiments.

Type 1. For the blockage model, only the control (no UV irradiation) subexperiment(s) were used to estimate the model parame-

TABLE 1
SUMMARY OF EXPERIMENTS, SUBEXPERIMENTS, AND OBSERVED YIELDS OF FORM-I SV40

Experiment	Subexperiment	Pulse duration	Dimers/genome	Observed yield of form I*
		min		*%*
1	1	15	0	100
—	2	15	2	29.8
2	1	16	0	100
—	2	12	0	38.5
—	3	8	0	15.8
—	4	16	3	16.0
3	1	16	0	100
—	2	8	0	23.0
—	3	16	2	33.0
—	4	16	3	18.3

*All yield values are expressed as a percentage of the yield for the unirradiated control sample of the longest pulse duration for each separate experiment.

ters (μ_R, σ_R, and L). Fits of type 1 were used to see how well the blockage model predicts the results of a subexperiment in which the infected cells had been irradiated using information based only on control data. For the slowdown model, these parameters (μ_R, σ_R, and L) referring to the behavior of the replication fork on unirradiated templates are shared with the blockage model and were fixed at the values estimated from the control data. The remaining slowdown model parameters, $\mu_s(\lambda)$ and $\sigma_s(\lambda)$, were then estimated from the subexperiment(s) in which infected cells had been irradiated. Figs. 2 and 3 and Tables II and III are based on these fits.

Type 2. In these fits, model parameters for the blockage or slowdown models were estimated using all subexperiments. There was no restriction imposed that the values of the parameters shared by the two models be equal. Fits of this type were used for formal comparisons between the fits of the two models (see next section).

A preliminary analysis comparing subexperiments performed at the same UV fluence showed that the variance of duplicate normalized fragment label intensities was roughly proportional to the square root of the observed label intensity. Thus, weights for least-squares fitting were chosen to be the reciprocal of the square root of the observation. To check the sensitivity of these results to the choice of weighting, alternative least-squares estimates were made with constant weights or weights equal to the reciprocal of the observation. In addition, a more general error structure was checked in which the error variance was modeled as a constant plus a power function of the expected fragment label intensity. These alternate methods gave nearly the same parameter values and identical qualitative answers in comparative model testing of the fits to the data. A set of FORTRAN subroutines computed the expected fragment label intensities for each model (see Appendix) and the derivative-free nonlinear regression program BMDPAR (Dixon, 1981) was used for the weighted least-squares fitting. Where needed, equality and inequality constraints were used (e.g., to prevent parameter estimates from being negative or during various tests of the models). Note that the lag parameter (see Appendix) can be estimated only if subexperiments were performed at different pulse-label durations, and the number of slowdown model parameters that can be estimated is a function of how many different UV fluences were studied.

Analysis of Model Fits

The adequacy of each model to predict the results of subexperiments in which infected cells were irradiated was assessed from type 1 fits by (a) visual inspection of their predictions (Fig. 3) and (b) by comparing the weighted residual sum of squares (WRSS equals the weighted sum of squared deviations between observed and predicted fragment label intensities) for a subexperiment to the expected WRSS if experimental error were the only source of deviation between observed and predicted fragment label intensities (Table II). Although there was no independent estimate of experimental error, an approximation was computed as follows. The observed fragment label intensities for subexperiments in which infected cells were irradiated with a UV fluence, which yields two dimers/genome (experiments 1 and 3), were compared, and the sum of the weighted variances of these duplicate values served as estimates of the expected WRSS from experimental error. Weights were the reciprocal of the square root of the mean fragment label intensity. Similar calculations were done for three dimers/genome using subexperiments from experiments 2 and 3. The expected WRSS from experimental error for two dimers/genome was based on data from nine restriction fragments (*Hind*II/III fragments E and F were not resolved on the gel in experiment 1) and was multiplied by ^{11}⁄$_9$ for comparison with the WRSS for experiment 3. A model prediction was considered adequate if the ratio of the WRSS for the predictions to the expected WRSS from experimental error was not markedly >1. An f test was used to judge statistical significance, although this is too conservative since the WRSS and expected WRSS are not independent. If the f tests were appropriate, then

TABLE II

COMPARISON OF WEIGHTED RESIDUAL SUMS OF
SQUARES (WRSS) TO EXPERIMENT ERROR (TYPE-1 FITS)

| Experiment | Dimers/genome | WRSS for predictions | | | Expected WRSS from experimental error§ |
| | | Blockage model | Slowdown models | | |
			(a)*	(b)‡	
1	2	50.6	152	80.7	41
2	3	154.3	99.2	21.5	25
3	2	26.4	158	83.2	50
3	3	34.5	189	59.9	25

*Slowdown model in which the coefficient of variation in the replication time has been constrained $[\sigma_t(\lambda)/\mu_t(\lambda) - \sigma_R/\mu_R]$.
‡Slowdown model in which the parameters $\mu_t(\lambda)$ and $\sigma_t(\lambda)$ were allowed to vary.
§Calculated as described in Analysis of Model Fits (see Methods).

considering the degrees of freedom for the numerator and denominator, a ratio >3 would be significant ($\alpha \simeq 0.05$).

Since the blockage and slowdown models are non-nested, classical procedures for comparing the fits of two models (e.g., f tests or likelihood ratio tests) are not appropriate. (Two models are nested if they have the same mathematical structure and if the parameter space for one model is a restriction or subset of the parameter space for the larger model.) We elected to use the Akaike Information Criterion (AIC; Akaike 1974, 1978) and the Schwarz Criterion (SC; Schwarz, 1978) to compare the performance of the two models, and these required model fits of Type 2. Details concerning the use of these methods are presented in the Appendix.

RESULTS

Development of Models

To develop mathematical models to predict the outcome of Danna and Nathans-type experiments following UV irradiation of SV40-infected cells, it was first necessary to define assumptions for the two general cases we considered. Justifications of some of these assumptions are presented in the Appendix.

Blockage Model. In this model, we propose that when a replication fork encounters a pyrimidine dimer in one of the template strands, strand elongation is blocked, and blocked molecules fail to complete replication during the course of the pulse label. Thus, any pyrimidine dimer in the unreplicated portion of a replicative intermediate or in any portion of a form-I molecule scheduled to enter the pool of replicative intermediates will prevent the genome from being recovered as a labeled completed form-I molecule. This is diagrammed in Fig. 1 a and c; here only half the circular SV40 genome is shown and the dimer is placed arbitrarily at its midpoint; completed form-I molecules are indicated by the brackets. Dimers in the previously replicated portions of replicative intermediates will not interfere with completion of these molecules. In this model, we assume that UV irradiation does not affect the rate of replication fork movement on dimer-free templates.

The location of pyrimidine dimers on the genome is assumed to be a Poisson process with parameter λ. Thus, if λ equals the mean number of dimers per complete genome and the entire genome is considered to have unit length, then the number of dimers within a stretch of double-stranded DNA of length x is distributed as Poisson with mean λx. Although nucleotide sequence variations may have a slight effect on the distribution of dimers on the genome, this is unlikely to have a significant effect on the main calculation derived from the Poisson assumption (i.e., the probability of at least one dimer in the unreplicated portion of the replicative intermediate).

Given these assumptions, the expected outcome of a Danna and Nathans-type experiment in which cells were irradiated with UV fluences yielding an average of one, two, and three dimers per genome and pulse labeled for a time equal to that required for one round of replication is shown schematically in Fig. 1 e. These curves can be compared with that of the unirradiated control ($\lambda = 0$). The predicted data have been normalized so that the area under each curve is proportional to the yeild of ^{3}H-label in completed form-I molecules. The bowed shape of the curves for the irradiated samples results from the enhanced labeling of terminal-proximal segments of the genome relative to origin-proximal segments. This occurs because there is a decreased probability that a dimer will occur ahead of the replication fork rather than behind the fork in molecules nearing completion at the time of irradiation. This steeper gradient of labeling of the dimer-containing population of molecules is superimposed on the normal gradient of labeling contributed by the dimer-free population.

Slowdown Model. In this model, we propose that dimers in DNA are not specific blocks to strand elongation, but that UV irradiation of infected cells causes an overall slowdown in the rate of replication fork movement. Thus, both dimer-free and dimer-containing molecules eventually become fully replicated but at a slower rate. We assume that the distribution of molecules within the pool of replicative intermediates is unchanged. In the example shown diagramatically in Fig. 1 f and g, replication fork movement in irradiated cells is occurring at half the rate as in unirradiated cells. Thus only 0.5 rounds of replication occur during the pulse labeling time and fewer molecules are completed. The curves predicted in a Danna and Nathans-type experiment following UV irradiation would resemble those obtained for shortened pulse-labeling times in unirradiated cells. Theoretical curves are drawn in Fig. 1 h for a unit (control) replication rate and for rates of replication fork movement reduced to 0.8, 0.6, and 0.4 times the normal rate. As would be expected, the curve for the unirradiated control is identical to that predicted in the case of the blockage model for $\lambda = 0$. As in Fig. 1 e, the areas under the curves are proportional to the predicted yields of form-I molecules.
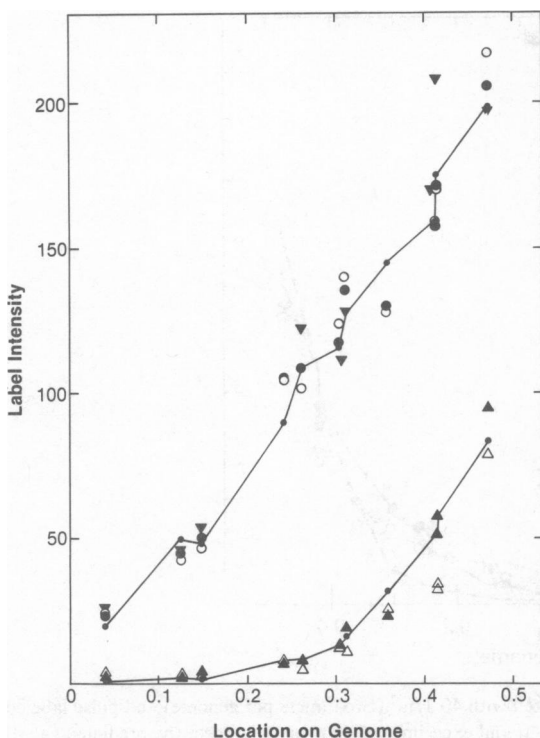
FIGURE 1 Schematic representation of models for UV-induced reduction in SV40 DNA synthesis. Only half of the bidirectionally replicated circular SV40 genome is represented; *ori* marks the origin of replication, *ter* marks the terminus. Dashed lines (---) indicate newly replicated ³H-labeled DNA. Brackets ([ ]) indicate completed molecules. (*a*) Molecules in the process of replication at *t* - 0 that contain dimers (●) in the template strand either ahead of or behind the replication fork. Dimers are shown in the center of the strand although they occur essentially at random along the strand. (*b*) The dimer-free population of molecules at *t* - 0. *Blockage model:* (*c*) The dimer-containing population of molecules after a pulse-labeling time equivalent to one round of replication in unirradiated cells. Molecules with the dimer behind the fork are completed; molecules with the dimer ahead of the fork are blocked. (*d*) The dimer-free population of molecules after a time equivalent to one round of replication in unirradiated cells. Molecules are replicated at the normal rate. (*e*) Label intensity in segments of completed molecules as a function of position on the SV40 genome; predicted curves for 0 (control), one, two, and three dimers per genome. *Slowdown model:* (*f*) The dimer-containing population of molecules after a time equivalent to one round of replication in unirradiated cells. Replication forks are not blocked by dimers but replication is slowed and only 0.5 round of replication has occurred. (*g*) The dimer-free population of molecules after a time equivalent to one round of replication in unirradiated cells. Molecules replicate at a reduced rate; only 0.5 rounds of replication has occurred. (*h*) Label intensity in segments of completed molecules as a function of position on the SV40 genome; predicted curves for unit replication rate (control) and for 0.8, 0.6, 0.4 times the normal rate. The label intensities plotted in *e* and *h* are normalized to the predicted yield of form-I molecules. Thus, the area under each curve is proportional to the yield of form I.

Refinement and Testing of Models

Three separate Danna and Nathans-type experiments (see Table I) were performed to provide a basis for refining and testing each of our two models for replication of SV40 DNA following UV irradiation. Included in these experiments were control subexperiments in which unirradiated SV40-infected cells were pulse labeled with ³H-thymidine for varying time periods, and subexperiments in which SV40-infected cells were UV irradiated with fluences yielding an average of either two or three dimers per genome (i.e., λ = 2 or 3). The control data were then used to predict values for our experimental results based on the two models. In the case of the slowdown model, additional

fitting was done based on our experimental results from UV-irradiated samples (see type 1 model fitting in the Model Fitting section).

The data from control subexperiments (λ = 0) presented in Fig. 2 are similar to those obtained by Danna and Nathans (1972). Here the label intensity or the ³H/³²P ratio in each SV40 *Hind* II/III restriction fragment is normalized to the total yield of ³H-label in form I and is plotted as a function of the mean distance of the fragment from the origin. The longest pulse-labeling time (label duration, $\bar{D}$ = 16 min) is approximately equal to the replication time for the genome. As expected, for a shorter labeling time ($\bar{D}$ = 8 min), there is overall reduction in the ³H-thymidine incorporated into completed molecules and

FIGURE 2 Control subexperiments in which unirradiated SV40-infected cells were mock treated and pulse labeled with ^{3}H-thymidine for 16 min (*upper curve*) and 8 min (*lower curve*). The data points shown are for experiments 1 (▼), 2 (O, △), and 3 (●, ▲); (●, O, ▼) indicate the observed fragment label intensities for the 16-min pulses; (▲, △), for the 8-min pulses. The lines (———) connect the values for the least-squares best fit of the data for experiment 3.

The results from subexperiments in which SV40-infected cells were UV irradiated are indicated by the symbols in Fig. 3. Here again the results from repeat experiments are in good agreement. As expected for either model, there is a marked UV fluence-dependent reduction in ^{3}H-label incorporation into completed molecules, and the label intensities of origin-proximal DNA fragments are reduced relative to those of origin-distal fragments.

Blockage Model. Values predicted by the blockage model for $\lambda = 2$ and $\lambda = 3$ are indicated by the solid lines in Fig. 3. The predictions shown here are from the blockage model with parameters μ_R, σ_R, and L estimated from the control subexperiments of experiment 3 (see above). It is evident from visual examination that predicted values fit well with the data from experiment 3 (closed circles). The predictions from the models, fit to the control subexperiments of experiments 1 and 2, are not shown in the figure. The WRSS between the observed data and the blockage model predictions for subexperiments from all three experiments are indicated in Table II. The WRSS provides us with a measure of the goodness of fit of each model to the experimental data; the lower the WRSS value, the better the fit. For three out of four subexperiments in which infected cells had been irradiated, these WRSS values are not significantly different from the WRSS values expected from experimental error (see Analysis of Model Fits in Methods). This indicates that the blockage model is able to adequately predict the outcome of a Danna and Nathans-type experiment performed following UV irradiation.

Slowdown Model. We next asked whether there were conditions under which the slowdown model would also allow a good approximation to our experimental data. We first tested this model under conditions where $\mu_s(\lambda)$ (mean slowed replication time; λ equals mean number of dimers per genome) and $\sigma_s(\lambda)$ (standard deviation in slowed replication time) were allowed to vary until a best fit with the experimental data was achieved, but the coefficient of variation $[\sigma_s(\lambda)/\mu_s(\lambda)]$ was constrained to equal that of control samples. The predicted values based on the fit to experiment 3 are indicated by the dashed lines in Fig. 3. For experiment 3, $\mu_s(2)$ (the estimated mean replication time in the slowdown model when $\lambda = 2$) is 32.6 min and $\mu_s(3) = 46.1$ min (Table III). It is clear from visual examination (Fig. 3) and WRSS values (Table II) that the fits for this form of the slowdown model are generally not as good as those for the blockage model.

Since the slowdown model has an intrinsic flexibility allowed by the two variables $\mu_s(\lambda)$ and $\sigma_s(\lambda)$, we next asked: If both of these were allowed to vary simultaneously, could we then achieve a good fit with our experimental data? For experiment 3 the best fit was achieved with $\mu_s(2) = 37.7$ min, $\sigma_s(2) = 12.4$ min, $\mu_s(3) = 58.0$ min, and $\sigma_s(3) = 19.2$ min (Table III and Fig. 3, dotted lines).
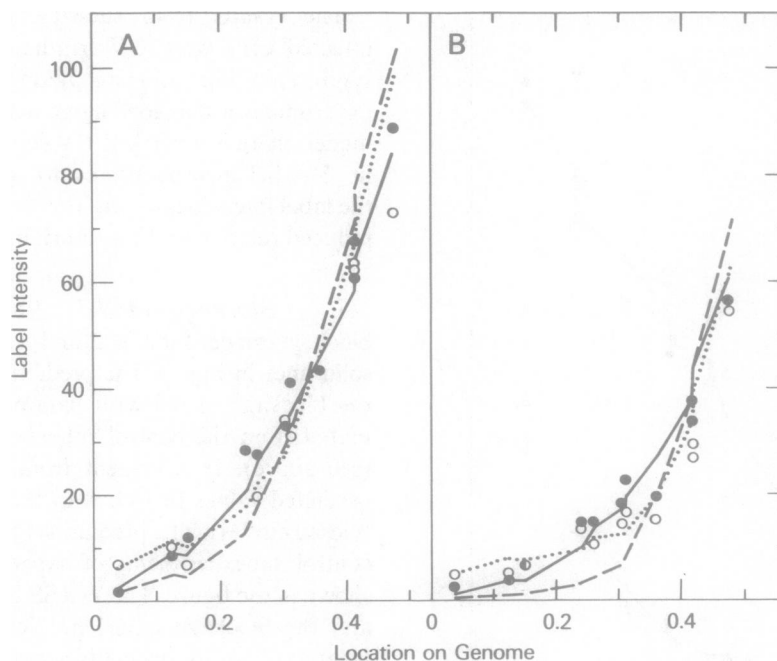
an increase in the ratio of origin-distal to origin-proximal label intensities. The results from the three repeat experiments for the longest pulse time are in very good agreement. The differences observed between the two repeats of the 8-min pulse are probably due to a slight change in the rapidity with which the samples were handled during the mock irradiation.

The presence of substantial amounts of label in origin-proximal DNA fragments after a short pulse label (8 min) may be indicative of a variability in the replication time for the SV40 genome. To incorporate this type of variability into our model, we assumed that the rate of replication fork progression is constant for each molecule but the rate varies among the molecules in the population (see Appendix); we also assumed a short delay in entry of label into the precursor pool (see below). An excellent fit to the control subexperiment data can be obtained when the parameters μ_R (mean replication time), σ_R (standard deviation of replication time), and L (delay in label incorporation) are estimated by weighted least squares. The solid lines in Fig. 2 connect the points for the best fit to the data from experiment 3 (●, ▲) with $\mu_R = 18.0 \pm 1.1$ min (estimate $\pm$ SE), $\sigma_R = 4.8 \pm 0.8$ min, and $L = 1.2 \pm 0.4$ min. The fits to the data from experiments 1 and 2 are similar and are not shown in the figure.

FIGURE 3   (*A*) Subexperiments in which SV40-infected cells were UV-irradiated with 40 J/m^2 (two dimers per genome) and pulse labeled with ^{3}H-thymidine for 16 min. The data points shown are from experiment 1 (O) and experiment 3 (●). Lines connect the predicted values assuming a blockage model (———) or slowdown models (---) and ($\cdot$ $\cdot$ $\cdot$). These fits were generated employing the parameters estimated from the least-square best fit of the control subexperiments for experiment 3. Additional parameters required for the slowdown curves, the slowed replication time (μ_s) and the slowed standard deviation (σ_s), are derived from a best fit of the subexperiment of experiment 3 in which infected cells were irradiated. We assumed a constant coefficient of variation in replication time (---) or no constraint on the slowed replication time or its standard deviation ($\cdot$ $\cdot$ $\cdot$). (*B*) Subexperiments in which SV40-infected cells were UV-irradiated with 60 J/m^2 (three dimers per genome) and pulse-labeled with ^{3}H-thymidine for 16 min. The data points are for experiment 2 (O) and experiment 3 (●). Lines connect the predicted values assuming either a blockage model (———) or slowdown models (---) and ($\cdot$ $\cdot$ $\cdot$). These predicted values were generated from least-squares best fit of experiment 3 as described in *A*.

TABLE III
PARAMETER ESTIMATES (TYPE-1 FITS)*

	Experiment 1			Experiment 2			Experiment 3		
	Blockage model	Slowdown models		Blockage model	Slowdown models		Blockage model	Slowdown models	
		(a)	(b)		(a)	(b)		(a)	(b)
μ_R§	16.9	16.9	16.9	16.4	16.4	16.4	18.0	18.0	18.0
σ_R‖	4.8	4.8	4.8	5.2	5.2	5.2	4.8	4.8	4.8
L¶	2‡	2‡	2‡	4.2	4.2	4.2	1.2	1.2	1.2
$\mu_s(2)$**	—	33.0	39.2	—	—	—	—	32.6	37.7
$\sigma_s(2)$‡‡	—	9.5	13.0	—	—	—	—	8.8	12.4
$\mu_s(3)$	—	—	—	—	47.1	57.4	—	46.1	58.0
$\sigma_s(3)$	—	—	—	—	14.9	19.1	—	12.4	19.2

*All estimates are expressed in minutes. Coefficients of variation for the parameters estimates range 10–33% for *L*, 5–24% for the μ parameters, and 5–60% for the σ parameters.

‡Lag parameter could not be estimated in experiment 1 because both subexperiments had identical pulse-label durations; *L* has been fixed at 2.

§μ_R equals the mean replication time.

‖σ_R equals the standard deviation in replication time.

¶*L* equals the lag time.

**$\mu_s(\lambda)$ equals the slowed mean replication time; λ is dimers per genome.

‡‡$\sigma_s(\lambda)$ equals the slowed standard deviation in replication time.

WRSS values for these fits are shown in Table II. In this case, the fits are better and appear to approach those of the blockage model. Thus we conclude that it is possible to derive a slowdown model in which the mean replication time is increased in a fluence-dependent fashion such that for three dimers per genome it takes an average of 1 h to complete replication and there is a large standard deviation in replication times.

Comparison of Models

The fits of type 1 described in Fig. 3 and Tables II and III provide us with an informal means to compare the fits of the blockage and slowdown model predictions to the experimental data. The WRSS values for these fits (Table II) demonstrate that the blockage model is able to provide the best fit of the data in three out of four subexperiments in which SV40-infected cells were UV irradiated. Thus, it appears that the blockage model is the better model for describing SV40 replication immediately after UV irradiation. However, formal statistical comparisons of these type 1 fits are difficult because different subexperiments were used for estimation of parameters for the two models.

To apply formal methods to compare model fits, it was necessary to use fits of type 2 in which data from all

subexperiments (control and irradiated) within an experiment were employed in the fitting process (see Methods). The results of these analyses of our model fits are presented in Table IV. The last two rows of Table IV in the first section entitled Comparison of model fits (type 2) summarize the AIC and the SC for comparisons among model fits. These methods are described in detail in the Appendix. Both criteria take into account the WRSS for each fit along with the number of data points (N) and model parameters (k). (WRSS values are higher for type 2 fits than type 1 fits because a greater number of data points are evaluated when all subexperiments within an experiment are fit simultaneously.) For each criterion, the model with the minimum value of the criterion function is considered the best model to explain the data. The minimum value for each criterion within an experiment can be found in Table IV.

For experiments 1 and 3, the WRSS and the AIC and SC criteria indicate that the blockage model provides the best fit of the experimental data. Furthermore, in the case of experiment 3, a conservative evaluation of the differences among the criteria for both models (see Appendix) strongly suggests that the blockage model could not be favored by chance alone. Although the slowdown model is favored in experiment 2, the differences among the information criteria may not be significant (see Appendix). This latter result may be attributable to technical difficul-

ties encountered in experiment 2 (see below). Again, for all three experiments, large values for the slowed replication times and their standard deviations are needed in order to achieve good fits with the slowdown model (Parameter estimates [type 2 fits], Table IV). In summary, the results of our formal comparisons of model fits also indicate that the blockage model is better able to describe the outcome of a Danna and Nathans-type experiment performed after UV irradiation than is the slowdown model.

In this context, note that we have reason to believe that experiments 1 and 3 were technically superior to experiment 2. The fractions of total label incorporated into form-I SV40 DNA in Hirt extracts of control samples (16-min pulse label) were significantly higher for experiments 1 and 3 (35–40% of total ^3H label was in form I) than for experiment 2 (only 15% was in form I) (data not shown). Since the Hirt extractions of infected cells for experiment 2 were not performed on ice, as in the case of experiment 3 (the experiment of comparable size), we presume that this reduction in the relative fraction of form I was the result of nonspecific nuclease activity in the Hirt extractions performed at room temperature. This factor may have contributed to the anomalously large values estimated for the lag parameter (L) for experiment 2 (Table III and the Parameter estimates [type 2 fits] section in Table IV). These values (4.2–4.3 min) are significantly higher than those estimated for experiment 3 (1.2–1.6

TABLE IV
BEST WEIGHTED LEAST-SQUARES FITS USING ALL SUBEXPERIMENTS

	Experiment 1 (2 subexperiments)			Experiment 2 (4 subexperiments)			Experiment 3 (4 subexperiments)		
	Blockage model	Slowdown model		Blockage model	Slowdown model		Blockage model	Slowdown model	
		(a)*	(b)‡		(a)	(b)		(a)	(b)
Comparisons of model fits (type 2)									
WRSS§	286.8	351.5	315.8	536.4	494.9	435.3	106.6	339.6	233.7
N	18	18	18	44	44	44	44	44	44
k	2	3	4	3	4	5	3	5	7
AIC	105.9	111.5	111.6	282.5	281.0	277.3	229.5	266.4	254.0
SC	107.6	114.2	115.2	287.9	288.1	286.3	234.8	275.3	266.5
Parameter estimates (type 2 fits)‖									
μ_R**	19.0	20.4	17.8	15.1	17.1	16.3	17.6	18.2	16.8
σ_R	5.5	6.6	4.5	4.7	5.6	5.2	4.4	5.7	4.1
L	0¶	0¶	0¶	4.3	4.3	4.2	1.2	1.6	1.3
$\mu_s(2)$	—	40.5	42.0	—	—	—	—	33.4	35.4
$\sigma_s(2)$	—	13.1	13.9	—	—	—	—	10.5	11.6
$\mu_s(3)$	—	—	—	—	49.5	57.3	—	46.8	54.7
$\sigma_s(3)$	—	—	—	—	16.2	19.0	—	14.7	18.2

*Slowdown model with coefficient of variation $\sigma_s(\lambda)/\mu_s(\lambda)$ constrained to equal σ_R/μ_R.
‡Slowdown model in which all parameters allowed to vary (no constraint).
§All abbreviations given are defined in text.
‖All estimates are expressed in minutes. Coefficients of variation for the parameter estimates range 7–31% for L, 4–19% for the μ parameters, and 9–67% for the σ parameters.
¶Lag parameter (L) could not be estimated in experiment 1 because both subexperiments had identical pulse-label durations; L has been fixed at 0.
**All symbols given are defined in the legend to Table III.

min) and for those determined from our measurements of the uptake and phosphorylation of ³H-thymidine under the conditions of these experiments (see below).

Do All Dimers Block?

Since our experimental data were best fit by the blockage model in which we assumed that all pyrimidine dimers in unreplicated regions block completion of replication, we next asked to what extent our data could be consistent with any accommodation of dimers during replication. If there were any significant rapid bypass of dimers (without the formation of discontinuities in daughter strands) during the pulse-labeling period, this would be equivalent to a reduction in the number of dimers per genome that serve as blocks. In particular, if we let λ be the true mean number of dimers induced per genome and p be the proportion of dimers ahead of replication forks that serve as blocks to completed replication (thus $1 - p$ is the proportion bypassed), then it is easy to show that this is equivalent to a blockage model in which the effective mean number of dimers/genome is $\lambda_e = p\lambda$. To estimate p, the data for each experiment were used for weighted least-squares fitting (type 2) by the blockage model after excluding λ as an independent variable and including λ_e among the estimable parameters. Then λ_e/λ serves as an estimate for p. The estimates and standard errors for p are summarized in Table V.

In all cases, p is close to one indicating that most, if not all, dimers ahead of forks serve as blocks. The deviations from 1 are not statistically significant ($\alpha = 0.05$) except for experiment 2. From the standard errors of our estimates of p, we have calculated the one-sided 95% confidence interval for p (see footnotes to Table V). From these values we can be extremely confident that <13% of the dimers ahead of replication forks can be rapidly bypassed. This value is

not significantly changed if we assume a 10% uncertainty in our calculations of the number of input dimers (λ).

Effect of UV Irradiation on Uptake and Phosphorylation of ³H-Thymidine

In the experiments described above, incorporation of ³H-thymidine into SV40 DNA is used as a measure of DNA replication. Since many of our conclusions rest on comparisons of label incorporation in UV irradiated and unirradiated cells, it is necessary to demonstrate that UV irradiation does not alter the kinetics of uptake and phosphorylation of ³H-thymidine in our system. We first measured the uptake of exogenously added ³H-thymidine into the acid-soluble fraction of SV40-infected cells after continuous pulse-labeling periods following UV irradiation at 60 J/m². The uptake of exogenous ³H-thymidine appears to exhibit the same kinetics in both irradiated and mock-treated samples (Figure 4 A). The level of ³H-label in the acid-soluble pool appears to reach a plateau value within 3 min after the initiation of the ³H-thymidine pulse. This level of intracellular ³H-label is maintained for up to two hours of pulse labeling in both mock-treated and irradiated samples (data not shown). The phosphorylation of ³H-thymidine was monitored by PEI-cellulose chroma-
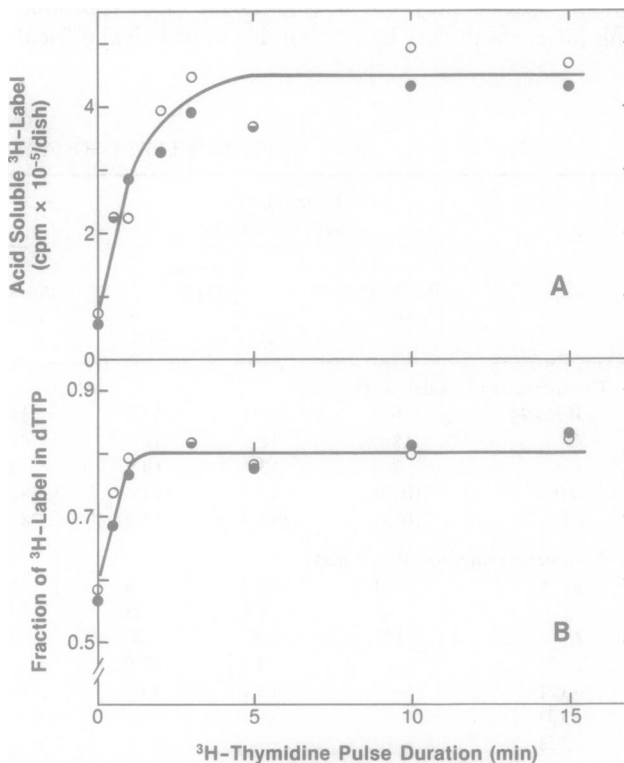

FIGURE 4 Uptake and phosphorylation of ³H-thymidine in mock-treated (●) and UV-irradiated (○) SV40-infected cells. (*A*) Uptake of ³H-thymidine was measured as described in Methods. Values are expressed as total acid-soluble ³H-cpm per dish of cells. (*B*) Phosphorylation of ³H-thymidine was measured by PEI-cellulose chromatography as described in Methods. Values are expressed as the fraction of total acid-soluble ³H-cpm migrating in the dTTP peak of a chromatogram.

TABLE V
ESTIMATES FOR THE PROPORTION (p) OF
DIMERS AHEAD OF FORKS THAT SERVE AS
BLOCKS TO SV40 DNA REPLICATION

Experiment	Dimers/genome*	Estimate‡ of p ± SE	One-sided 95% confidence interval§ for p
1	2	1.07 ± 0.11	≥0.88
2	3	1.22 ± 0.10	≥1.05
3	2	0.93 ± 0.04	≥0.87
3	3	1.03 ± 0.05	≥0.95

*Number of dimers per genome (λ) based on calculations of the rate of dimer formation as a function of UV fluence under our experimental conditions (see Methods).

‡Estimated by weighted least-squares using the blockage model and including λ_e (the effective mean number of dimers per genome) among the estimable parameters.

§The estimate of λ_e divided by λ (second column) is an estimate of p. Using asymptotic theory, one can be 95% confident that the true proportion is ≥ (estimate) − 1.645 × SE.

tography of aliquots of the same cellular acid extracts. In both mock-treated and UV-irradiated samples, ^{3}H-thymidine is rapidly phosphorylated such that within 3 min ~80% of the acid-soluble radioactivity is found in dTTP (Fig. 4 B); this percentage remains essentially unchanged for pulse-labeling periods up to 2 h (data not shown).

The total intracellular concentration of dTTP was determined by preparing acid extracts and measuring dTTP in a DNA polymerase assay (see Methods). Table VI summarizes the results of these assays for various periods of pulse labeling with nonradioactive thymidine. The 10-min pulse immediately after UV irradiation was chosen as an appropriate period after which to measure the total intracellular dTTP pool for the purpose of interpreting the experiments described in this paper. The total intracellular concentration of dTTP in these samples appears unchanged following UV irradiation.

Since we observe little or no effect of UV irradiation on the uptake or phosphorylation of ^{3}H-thymidine nor on the size of the intracellular dTTP pool, these experiments appear to validate our use of ^{3}H-thymidine uptake as a measure of DNA replication in UV irradiated and unirradiated cells.

DISCUSSION

We have tested two general models for the inhibition of DNA replication immediately following UV irradiation. In the blockage model, pyrimidine dimers in the templates are specific blocks to the completion of SV40 DNA replication; in the slowdown model, UV irradiation causes a nonlesion-specific slowdown in DNA replication on all molecules. Our experiments indicate that the blockage model is better able to predict the outcome of a Danna and Nathans-type experiment performed with UV irradiated SV40-infected cells than is the slowdown model. The slowdown model is able to fit the data only when its extra parameters, $\mu_s(\lambda)$ and $\sigma_s(\lambda)$, are allowed to vary. The result of this fitting process is the estimation of marked UV fluence-dependent increases in the slowed replication times and their standard deviations. The estimation of these wide distributions in replication times following UV irradiation could be indicative of lesion-specific effects on the completion of SV40 DNA replication. Thus, this version of the

TABLE VI
INTRACELLULAR dTTP AFTER UV IRRADIATION OR MOCK TREATMENT OF SV40-INFECTED CELLS*

Pulse time	UV irradiated (60 J/m^2)	Mock irradiated
min		
0–10	55.3	58.3
30–60	73.0	84.4
120–150	53.2	54.5

*Total intracellular dTTP (picomoles per milligram of cell protein).

slowdown model might be expected to be almost indistinguishable from the blockage model. However, note that despite this intrinsic flexibility of the slowdown model, the more parsimonious blockage model still provides the better fit of the experimental data. Our finding that the effects of UV irradiation on DNA replication are not readily explained by an overall slowing of replication fork movement is consistent with previous measurements of strand elongation in UV irradiated cells by a bromodeoxyuridine photolysis method (Povirk and Painter, 1976).

Given only the replication parameters (μ_R, σ_R, and L) and the pyrimidine dimer content of the molecules, the blockage model can be used to accurately predict values for the normalized label intensities of restriction fragments in newly completed pulse-labeled SV40 molecules. Because label intensity values have been normalized to reflect the total incorporation of label into form I for each sample, this good fit of the blockage model predictions to the experimental data indicates that blockage of strand elongation by pyrimidine dimers can fully account for the reduction in form-I SV40 DNA synthesis after irradiation of infected cells. In addition, we can conclude that few, if any, of the dimer sites in the DNA are rapidly bypassed allowing completion of molecules within the normal replication time. Thus, blockage (or interruption) in strand elongation appears to occur independently of the strand on which the dimer is found (whether it be on the forward or the retrograde strand template). Blockage in strand elongation by pyrimidine dimers is consistent with in vitro studies that show that DNA synthesis by polymerase α stops one nucleotide before potential dimer sites on UV-irradiated ϕX174 templates (Moore et al., 1981). Recent work in our laboratory indicates that replication forks do not halt or pause at pyrimidine dimer sites, instead strand elongation is interrupted and the site is bypassed, leaving gaps that require additional time for filling (White and Dixon, 1984).

Previous studies in which DNA fiber autoradiography was used to measure replication fork movement in mammalian cells immediately after UV irradiation have shown that the average length of labeled DNA segments is decreased in a UV fluence-dependent fashion (Edenberg, 1976; Dahle et al., 1980). These results have been interpreted to indicate that pyrimidine dimers in DNA specifically block replication fork progression. However, direct quantitation of the relative effects of blockage and inhibition of initiation of replicons is impossible in these studies, and it is also impossible to determine whether or not a significant proportion of the replication forks are able to rapidly bypass dimers in template strands with or without the formation of gaps (gaps of <4,000 bases cannot be detected by DNA fiber autoradiography). Doniger (1978) concluded from additional fiber autoradiography studies that replication forks do bypass dimers, but strand elongation is interrupted at dimer sites leaving gaps in daughter strands. The conclusion that pyrimidine dimers specifically

block DNA strand elongation in mammalian cells has also been drawn from alkaline sucrose gradient analyses of the size of newly synthesized DNA (Lehmann, 1972; Doniger, 1978). The average size of these newly synthesized strands appears to correlate with the interdimer distance on the template strands.

Interpretation of both types of studies described above is complicated by the complexity of the cellular genome. Since the observed results are an average of the effects of UV irradiation on a heterogeneous population of replicons, it is very difficult to draw precise quantitative conclusions. In contrast, we have demonstrated here, that the SV40 replicon provides a system in which the effects of UV irradiation on DNA replication in mammalian cells can be studied in quantitative terms. This system is simple and sufficiently well defined so that precise mathematical models can be developed to describe replication of the SV40 molecules and its perturbation by UV irradiation. These models are presently being extended to include the cumulative effects of UV damage at later times after UV irradiation.

All of the Danna and Nathans-type experiments considered here have been performed immediately following UV irradiation (0–16 min). Other studies in our laboratory have demonstrated that, at later times after UV irradiation (0.5–3 h), dimers are somehow accommodated by the cell's replication machinery so that dimers begin to appear in newly replicated completed (form I) molecules (Stacks et al., 1983). This suggests either that dimers only cause a delay in completion of replicating molecules or that the probability a dimer will serve as a block to replication decreases at later times following irradiation. The mechanism(s) by which dimers are accommodated at these later times is being investigated currently in our laboratory.

APPENDIX

Here we describe the mathematical models developed for the expected labeling of DNA fragments from restriction cleavage after pulse labeling with ^{3}H-thymidine. We also include information regarding the use of the Akaike and Schwarz criteria to compare model fits. The Appendix material serves as a supplement to the information found in the text.

Modeling Assumptions

Restriction Fragment Position and Size. The SV40 map used for the specification of *Hind*II/III fragment boundaries (see Table VII) was derived from SV40 sequence data (Fiers, 1978). The total map length is normalized to 1.0 with the origin at map position 0. Proceeding from the origin in the direction of late transcription, positions of boundaries are indicated in map units from the origin with suffix L; those in the direction of early transcription from the origin receive a suffix E. The terminus is thus labeled as both 0.5L and 0.5E. Table VII summarizes for each fragment its map length and percent adenine-thymine (A-T) composition (both determined from the DNA sequence) in order of increasing average absolute distance from the origin. For all fragments other than C and G, this distance is the map length from the origin to the midposition of the fragment. Since fragments C and G straddle, respectively, the origin and terminus, their average absolute distances from the origin are computed as the weighted average of the distances from the

TABLE VII
SUMMARY OF SV40 DNA *HIND*II/III
FRAGMENTS*

Fragment	Average absolute distance of fragment from origin‡	Map boundaries relative to origin‡	Length‡	A-T composition
				%
C	0.0400	0.0137E–0.0900L	0.1037	48.71
A	0.1252	0.0137E–0.2367E	0.2230	63.30
D	0.1495	0.0994L–0.1995L	0.1001	55.81
E	0.2422	0.1995L–0.2848L	0.0853	59.06
H	0.2622	0.2367E–0.2876E	0.0509	65.54
K	0.3053	0.2848L–0.3258L	0.0410	57.21
I	0.3123	0.2876E–0.3370E	0.0494	61.78
F	0.3591	0.3258L–0.3923L	0.0665	59.60
B	0.4141	0.3370E–0.4911E	0.1541	60.77
J	0.4154	0.3923L–0.4385L	0.0462	55.37
G	0.4726	0.4385L–0.4911E	0.0704	59.62
			0.9906	

*Derived from sequence data (Fiers, 1978).
‡Distances expressed as fraction of total genome length; E and L indicate direction of early and late transcription, respectively.

origin for the early and late portions of the fragment. Notice that all lengths do not quite add up to 1.00 since there are unrecovered fragments between C and D of length 0.009.

Since different strains of SV40 virus are known to differ slightly, we estimated fragment lengths and relative A-T compositions for our SV40 virus stock in experiments in which we digested SV40 DNA, uniformly labeled with ^{32}P or ^{3}H (data not shown). In general, these estimates agree well with those computed from the sequence data.

Uniform Replication Fork Movement. For these models, we assume that in a cohort of unirradiated virus with replication time, R min, the speed of replication fork movement in replicative intermediates (RI) is constant (nonrandom), and both forks proceed from the origin to the terminus with speed $0.5/R$ map units/min. It is assumed that there is no significant use of alternate origins of replication (Martin and Setlow, 1980), and there is no lag between the time the fork reaches the terminus and the release of completed form-I viral DNA.

Although there is some evidence for nonconstant fork movement in replicative intermediates (i.e., slowed movement during termination phase [Tapper and DePamphilis 1978]), the assumption of constant and symmetric fork movement appears reasonable as a first-order approximation. Any fixed lag during termination would be equivalent to an effective net shortening of the pulse-label duration (see the Delay in Label Entry section). Analyses of replicative intermediates produced in unirradiated cells reveals no significant subpopulation of viral genomes with asymmetrically advancing forks (Tapper and DePamphilis, 1980). In addition, we have shown recently that replication fork asymmetry is not observed following UV irradiation of SV40-infected cells (White and Dixon, 1984).

Stochastic Variations in Replication Times. Assuming that individual RIs have constant rates of fork movement, but that the population of rates is variable, allows for a population approach to the modeling of nonconstant fork movement. Any stochastic variation in observed replication times of unirradiated viruses is modeled by assuming a truncated Gaussian distribution for R with mean μ_R and standard deviation σ_R. The density function is truncated to be zero outside the region $\mu_R \pm 3\sigma_R$, and it is assumed that σ_R is $<\mu_R/3$. A more correct

mechanistic explanation of the variability in population replication times would probably assume a random speed of fork movement in individual RIs (e.g., through multiple stopping and starting of fork movement), but this approach is mathematically less tractable. However, since the data analysis assesses total label intensities in a population of fragments, a more detailed stochastic analysis might not offer any significant advantage.

The use of a truncated Gaussian and constraint on σ/μ is to permit the simple specification of the functional form of the density function using just two parameters (mean and standard deviation) and to avoid the possibility of nonpositive replication times. The choice of this distribution over other biologically reasonable positive unimodal distributions was fairly arbitrary, and was mainly decided on the basis of ease of coding and specification. Another reasonable consideration would be a gamma distribution for R or even a gamma distribution for the speed of replication $0.5/R$ (see below).

No Reentry of Labeled Molecules. The duration of labeling is short enough that one can ignore the return of labeled completed form-I molecules back into the RI pool. Since only completed form-I molecules were recovered in these experiments and the duration of pulse label was never greater than the mean replication time, it is unlikely that a DNA molecule in the RI pool at the start of the pulse label will have daughters that also complete replication during the pulse.

Definition of Replication Cycle Index, s. For a cohort of unirradiated viral genomes with replication time, R, the maturity or cycle age of each viral genome can be represented by the replication cycle index, s; this number is the location of either fork in map units from the origin if the viral genome is in the RI pool, or is equal to $-0.5w/R$ for form-I genomes that have w min to go before entering the RI pool. Notice that $0 < s < 0.5$ indicates a viral genome in the RI pool, $2s$ being the fraction of the genome already replicated, and $s < 0$ indicates a form-I genome. In the absence of UV irradiation, a viral genome at index s at time 0 is at index $s + t (0.5/R)$ at time t. Value of $s > 0.5$ indicate that the viral genome has left the RI pool and is recoverable as a completed form I.

Uniform Distribution of s. If K is a positive constant such that no viral genome with replication cycle index $s < -K$ at the start of the pulse label is potentially recoverable as a labeled form I at the end of the pulse, then at the time of pulse labeling a dynamic equilibrium is reached such that the distribution of s is uniform on the interval $(-K, 0.5)$. A uniform distribution for s follows if one assumes a steady state RI pool size has been reached (rate of entry equals rate of exit). There is some difficulty in interpreting this distribution for $s < 0$, but for $0 < s < 0.5$, there is experimental evidence to support the nearly uniform distribution of replication fork location (except possibly during terminal events as discussed above; Tapper and DePamphilis, 1980).

Delay in Label Entry. Any delay in the availability of label to the precursor nucleotide pool (resulting from manipulation of the cells or lag in uptake or phosphorylation of ^{3}H-thymidine) is modeled simply by assuming an effective net shortening of the pulse duration. Experimental results show that the thymidine label is 80% equilibrated in the dTTP pool within 2–3 min. This minor lag was modeled by a simple delay in the effective pulse duration.

Mathematical Models

Blockage Model. In a cohort with constant replication time R, $\tilde{D}$ equals the pulse duration; L, the lag in label incorporation; $D = \tilde{D} - L$, the effective pulse duration; and λ, the mean number of induced UV hits per genome. Before irradiation, the proportion of the cohort with replication cycle index between s and $s + ds$ is by the uniform distribution

of s

$$\tilde{P}(s)\mathrm{d}s = 2c\,\mathrm{d}s, \qquad -K \le s \le 0.5 \tag{A1}$$

where $c = 0.5/(0.5 + K)$.

After UV irradiation RIs, with pyrimidine dimers in unreplicated portions, and form Is, with any dimers, will drop out from the recoverable pool. The proportion of the cohort with index between s and $s + ds$ with no dimers ahead of the fork (or no dimers if $s < 0$) is by the assumption of a Poisson process with parameter λ

$$P(s, \lambda)\mathrm{d}s = \begin{cases} 2c\exp[-\lambda(1 - 2s)]\mathrm{d}s, & 0 \le s \le 0.5 \\ 2c\exp(-\lambda)\mathrm{d}s, & -K \le s < 0. \end{cases} \tag{A2}$$

To have label incorporation at position s on the genome, the replication index must be $<s$ when the pulse label starts but $>0.5 - D(0.5/R)$ to have recovery in completed form-I genomes. Thus, the proportion of the cohort that is recovered as completed form Is with label at position s $(0 \le s \le 0.5)$ is equal to

$$Q(s, D, R, \lambda) = \begin{cases} \int_{0.5(1-D/R)}^{s} P(x, \lambda)\mathrm{d}x, & s \ge 0.5(1 - D/R) \\ 0, & s < 0.5(1 - D/R). \end{cases} \tag{A3}$$

Carrying out the integration

$$Q(s, D, R, \lambda) = \begin{cases} c(e^{-\lambda}/\lambda)(e^{2\lambda s} - e^{\lambda(1-D/R)}), \\ \quad 0 \le 0.5(1 - D/R) \le s, \quad \lambda > 0 \\ ce^{-\lambda}[(e^{2\lambda s} - 1)/\lambda + D/R - 1], \\ \quad 0.5(1 - D/R) \le 0 \le s, \quad \lambda > 0 \\ c(2s - 1 + D/R), \\ \quad 0.5(1 - D/R) \le s, \quad \lambda = 0 \\ 0, \qquad \text{otherwise.} \end{cases} \tag{A4}$$

Finally, if the boundaries of fragment j extend from position s_{1j} to position s_{2j} ($s_{1j} < s_{2j}$, and both on same side of the origin), the tritium label recovered in all copies of this fragment from completed form Is will be proportional to $A_j \int_{s_{1j}}^{s_{2j}} Q(x, D, R, \lambda)\,\mathrm{d}x$, where A_j is the proportion of thymidine in the fragment (Table VII), assumed to be uniformly distributed over the fragment. Letting $s_{ij}^* = \max[s_{ij}, 0.5(1 - D/R)]$, the label for each fragment is proportional to

$$I_j(D, R, \lambda) = \begin{cases} c(A_j/\lambda)(e^{\lambda(2x-1)}/2\lambda - xe^{-\lambda D/R})\big|_{x-s_{1j}^*}^{s_{2j}^*}, \\ \quad D/R \le 1, \quad \lambda > 0 \\ c(A_j/\lambda)\{e^{\lambda(2x-1)}/2\lambda \\ \quad - x[1 + \lambda(1 - D/R)]e^{-\lambda}\}\big|_{x-s_{1j}^*}^{s_{2j}^*}, \\ \quad D/R > 1, \quad \lambda > 0 \\ cA_j[x^2 - x(1 - D/R)]\big|_{x-s_{1j}^*}^{s_{2j}^*}, \\ \quad \lambda = 0. \end{cases} \tag{A5}$$

The integration for fragments straddling the origin or terminus are carried out separately for their right and left halves and then combined.

Slow-Down Model. The mathematics for the slowdown model is equivalent to that for the blockage model with $\lambda = 0$ but for longer replication times. In this model, a cohort of irradiated viral genomes will have an effective increased replication time, S, with label for each fragment $I_j(D, S, 0)$ in eq. A5.

Stochastic Modeling. As a first approximation to modeling biologic variability in replication rates, it is assumed that there is a

distribution in the number of viral particles having replication time R, the cohort with replication times between R and $R + dR$ having a constant speed $0.5/R$ for replication fork movement. For a specified mean μ_R and standard deviation σ_R, the following truncated Gaussian density function is used

$$f(R) = \begin{cases} c_1 \exp \{-0.5[(R - \mu_R)/c_2\sigma_R]^2\}, \ |R - \mu_R| \leq 3\sigma_R \\ 0, \text{ otherwise}, \end{cases} \quad (A6)$$

where $c_1 = 0.9879397917/(2\pi)^{1/2}\sigma_R$ and $c_2 = 1.015386985$. Thus, the expected value of the jth fragment tritium labeling is

$$E_j(D, \lambda, \mu_R, \sigma_R) = \int_{-\infty}^{\infty} I_j(D, R, \lambda) f(R) dR \quad (A7)$$

and the expected total yield is $\Sigma_j E_j(D, \lambda, \mu_R, \sigma_R)$. The proportionality constant c in Eq. A5 is rescaled to make the expected total yield equal 100 for the control subexperiment of longest pulse-label duration. For all subexperiments, the predicted label intensity (thymidine label per size) for fragment j is $E_j(D, \lambda, \mu_R, \sigma_R)$ divided by the map length of fragment j.

For the slowdown model, in addition to specifying μ_R and σ_R for the unirradiated case, one must specify the mean $\mu_s(\lambda)$ and standard deviation $\sigma_s(\lambda)$ for the increased replication times in the irradiated case at a specific UV dose λ, and use $\lambda = 0$ in Eq. A7.

Note that if we use the random variable $V = 0.5/R$, then the random variable terms in Eq. A5 would only contain powers of V and $\exp(-V)$. Then, if V were to have a gamma distribution, the expected total label for each fragment could be expressed in closed form, in part including several terms of incomplete gamma functions because of the boundary conditions. However, preliminary numerical trials demonstrated that integration of Eq. 7 using Simpson's rule with 30 intervals over the domain of the truncated Gaussian would often give at least 4 digits accuracy (of course under the assumption of R being a truncated Gaussian). This coding was sufficiently easy and the computer runs sufficiently fast so that it was not necessary in the present study to explore the closed form solutions involving V as a random variable or to explore other quadrature rules for the truncated Gaussian that might require fewer numerical operations.

Analysis of Model Fits (Type 2)

In the case where rival models of differing dimensionality (number of parameters) are being compared, it is possible that an incorrect model may fit the data at least as well as the correct model simply because the incorrect model has more adjustable parameters. The AIC and SC methods were designed to pick the correct model in this context under conditions of maximum likelihood estimation. In essence, each method evaluates a criterion function equal to the sum of a measure of a model's fit (minus twice log maximum likelihood) and a penalty function proportional to the number of parameters required to achieve the fit; the model with the minimum criterion value is considered the most appropriate model to describe the data.

If $WRSS_j$ is the least-squares WRSS for model j with k_j independently adjusted parameters, then under the assumption of Gaussian uncorrelated errors and correctly chosen weights (up to an unknown proportionality constant), the AIC for model j becomes $AIC_j = N \ln (WRSS_j) + 2 k_j$, where N is the total number of data points. The model with the smallest AIC_j can be considered the best model from the perspective of information theory. Notice that a model with a lower WRSS might be less favored if it achieved this reduction at the expense of parsimony (i.e., by having too many parameters). The Schwarz criterion has a somewhat different derivation but the same interpretation. The SC for model j is $SC_j = N \ln (WRSS_j) + \ln (N)k_j$, and again the model with the smallest value is considered best.

The AIC and SC procedures are generally used for decision making based simply on which model has the smallest criterion value. There is no analytic theory for the distribution of differences between criteria for

non-nested models, and it is not possible to state the statistical significance of differences among the criteria. Nevertheless, one can develop a rough idea of how different the criteria must be in order to be confident that the model with the smallest criterion value was not picked by chance alone. A highly conservative estimate can be obtained by noting that the standard error of $N \ln (WRSS_j)$ is approximately $N \sqrt{2/(N - k_j)}$, if the model fit adequately reflects experimental error and errors are Gaussian; for experiments 1, 2, and 3 these standard errors are 6.5, 10, and 10, respectively. If the $WRSS_j$ were independent, it would be unlikely that differences between the criteria >2.8 times the standard error could occur by chance alone ($P < 0.05$), and since the $WRSS_j$ are highly correlated, the real significance level would be much smaller. For example, in experiment 3, the information criteria for the blockage model are at least 25–32 units smaller than those of the rival slowdown model, and with the above calculations a difference of 28 would be unlikely to occur by chance alone. When these criteria are applied to nested models for which significance levels can be computed, differences between criteria >2 may be significant.

REFERENCES

Akaike, H. 1974. A new look at the statistical model identification. *IEEE (Inst. Electr. Electron. Eng.) Transactions on Automatic Control.* AC-19:716–723.

Akaike, H. 1978. A Bayesian analysis of the minimum AIC procedure. *Ann. Inst. Statist. Math.* 30:9–14.

Dahle, D., T. D. Griffiths, and J. G. Carpenter. 1980. Inhibition and recovery of DNA synthesis in UV-irradiated Chinese hamster V-79 cells. *Photochem. Photobiol.* 32:157–165.

Danna, K. J., and D. Nathans. 1972. Bidirectional replication of simian virus 40 DNA. *Proc. Natl. Acad. Sci. USA.* 69:3097–3100.

DePamphilis, M. L., and P. M. Wassarman. 1982. Organization and replication of papovavirus chromosomes. *In* Organization and Replication of Viral DNA. A. S. Kaplan, editor. CRC Press Inc., Boca Raton, FL. 37–114.

Diggelmann, H., and P. Beard. 1976. Growth and purification of SV40 and polyoma virus. *In* Animal Virus Course. Cold Spring Harbor Laboratory, Cold Spring Harbor, New York. 5–6.

Dixon, W. J. 1981. BMDP Statistical Software. University of California Press, Berkeley. 733.

Doniger, J. 1978. DNA replication in ultraviolet light-irradiated Chinese hamster cells: the nature of replicon inhibition and post-replication repair. *J. Mol. Biol.* 120:433–446.

Edenberg, H. J. 1976. Inhibition of DNA replication by ultraviolet light. *Biophy. J.* 16:849–860.

Edenberg, H. J. 1983. Inhibition of simian virus 40 DNA replication by ultraviolet light. *Virology.* 128:298–309.

Fiers, W. R., G. Contreras, G. Haegeman, R. Rogiers, A. Van der Voorde, H. van Heuverswyn, J. van Herreweghe, G. Volckaert, and M. Ysebaert. 1978. The complete nucleotide sequence of SV40 DNA. *Nature (Lond.).* 273:113–120.

Garrett, C., and D. V. Santi. 1979. A rapid and sensitive high pressure liquid chromatography assay for deoxyribonucleoside triphosphates in cell extracts. *Anal. Biochem.* 99:268–273.

Hall, J. D., and D. W. Mount. 1981. Mechanisms of DNA replication and

mutagenesis in ultraviolet-irradiated bacteria and mammalian cells. *Prog. Nucl. Acid Res. Mol. Biol.* 25:53–126.

Hand, R. 1976. Thymidine metabolism and DNA synthesis in Newcastle disease virus-infected cells. *J. Virol.* 19:801–809.

Hirt, B. 1967. Selective extraction of polyoma DNA from infected mouse cell cultures. *J. Mol. Biol.* 26:365–369.

Jagger, J. 1967. Potassium ferrioxalate actinometry. *In* Introduction to Research in Ultraviolet Photobiology. Prenctice-Hall, Inc., Englewood Cliff, New Jersey. 137–139.

Lehmann, A. R. 1972. Post-replication repair of DNA in ultraviolet-irradiated mammalian cells. *J. Mol. Biol.* 66:319–337.

Lindberg, U., and L. Skoog. 1970. A method for the determination of dATP and dTTP in picomole amounts. *Anal. Biochem.* 34:152–160.

Lowry, O. H., N. J. Rosebrough, A. L. Farr, and R. J. Randall. 1951. Protein measurement with the Folin phenol reagent. *J. Biol. Chem.* 193:265–275.

Martin, R. G., and V. P. Setlow. 1980. The initiation of SV40 DNA synthesis is not unique to the replication origin. *Cell.* 20:381–391.

Moore, P. D., K. K. Bose, S. D. Rabkin, and B. S. Strauss. 1981. Sites of termination of *in vitro* DNA synthesis on ultraviolet and *N*-acetylaminofluorene-treated ϕX174 templates by prokaryotic and eukaryotic DNA polymerases. *Proc. Natl. Acad. Sci. USA.* 78:110–114.

Povirk, L. F., and R. B. Painter. 1976. Rate of DNA chain elongation in ultraviolet light-irradiated mammalian cells as estimated by a bromodeoxyuridine photolysis method. *Biophys. J.* 16:883–889.

Randerath, K., and E. Randerath. 1968. Thin-layer separation methods for nucleic acid derivatives. *Methods Enzymol.* 12A:323–347.

Robb, J. A., and K. Huebner. 1973. Effect of cell chromosome number on simian virus 40 replication. *Exp. Cell Res.* 81:120–126.

Sarasin, A. R., and P. C. Hanawalt. 1980. Replication of ultraviolet-irradiated simian virus 40 in monkey kidney cells. *J. Mol. Biol.* 138:299–319.

Schwarz, G. 1978. Estimating the dimension of a model. *Annals of Statistics.* 6:461–464.

Shenk, T. E., J. Carbon, and P. Berg. 1976. Construction and analysis of viable deletion mutants of simian virus 40. *J. Virol.* 18:664–671.

Stacks, P. C., J. H. White, and K. Dixon. 1983. Accommodation of pyrimidine dimers during replication of UV-damaged SV40 DNA. *Mol. Cell. Biol.* 3:1403–1411.

Tapper, D. P., and M. L. DePamphilis. 1978. Discontinuous DNA replication: Accumulation of simian virus 40 DNA at specific stages in its replication. *J. Mol. Biol.* 120:401–422.

Tapper, D. P., and M. L. DePamphilis. 1980. Preferred DNA sites are involved in the arrest and initiation of DNA synthesis during replication of SV40 DNA. *Cell* 22:97–108.

White, J. H., and K. Dixon. 1984. Gap filling and not replication fork progression is the rate-limiting step in the replication of UV-damaged simian virus 40 DNA. *Mol. Cell. Biol.* 4:1286–1292.

Williams, J. I., and J. E. Cleaver. 1978. Perturbations in simian virus 40 DNA synthesis by ultraviolet light. *Mutat. Res.* 52:301–311.